Supplementary Information (SI) for Soft Matter.

Supporting Information for Investigating Glass Transition in PA6T/66 Copolymer through Molecular Dynamics Simulations

Lele Wei, Liping Zhu, Jin Wen* and Meifang Zhu
State Key Laboratory of Advanced Fiber Materials,
College of Materials Science and Engineering, Donghua University, Shanghai 201620, China

1 Computational Details

Intermolecular interactions in PA6T by the PCFF prediction, for π–π interactions, we varied the distance between two parallel benzene rings from 3.0 Å to 8.0 Å in increments of 0.5 Å, and calculated the total energy of the system at each distance. The π–π interaction energy was then obtained by subtracting the energies of the two individual monomers from the total energy of the interacting dimer system, as shown in Figure S4(a). For hydrogen bonding interactions, we varied the distance between the hydrogen atom of the amide group and the oxygen atom of a neighboring carbonyl group from 1.5 Å to 3.0 Å in increments of 0.1 Å. Similarly, the interaction energy was determined by subtracting the energies of the two individual monomers from the total energy of the interacting dimer system, as shown in Figure S4(b).

Table S1: Amorphous copolymer models of PA6T/66.

System	Chains	PA6T repeat units/Chain	PA66 repeat units/Chain	PA6T molar ratio
P-45	10	9	11	45%
P-50	10	10	10	50%
P-55	10	11	9	55%
P-60	10	12	8	60%

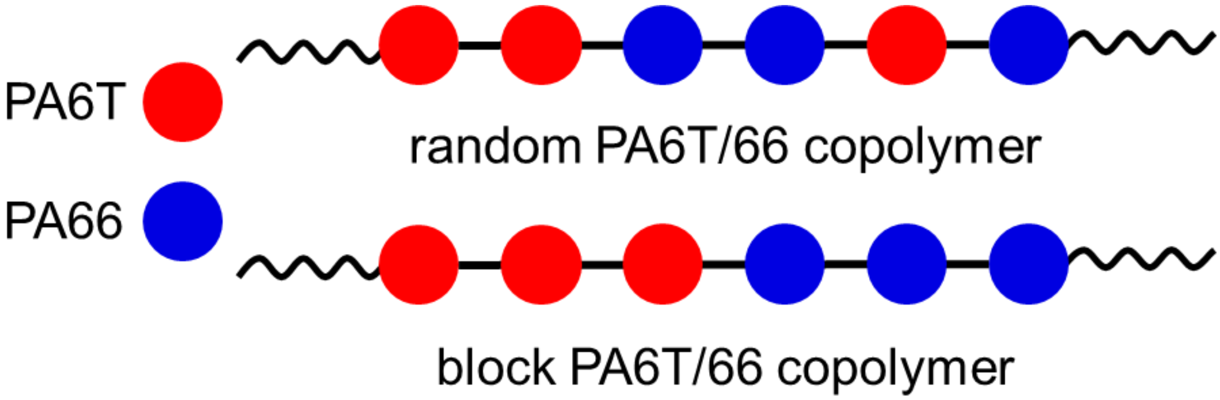

Figure S1: Structures of PA6T/66 random and bolck copolymers.

Table S2: Atom numbering, atom type and atomic charges of PA6T/66.

Numbering	Type	Charge (e)
1	HN	0.2487
2	NA	-0.5801
3	C2	-0.0233
4	HC	0.0530
5	C2	-0.1060
6	C2	0.1040
7	N_2	-0.6990
8	HN2	0.3780
9	C_1	0.6600
10	O_1	-0.5310
11	CP	-0.0180
12	CP	-0.1268
13	HC	0.1268
14	C_1	0.6420
15	C_1	0.7020
16	O_2	-0.5940

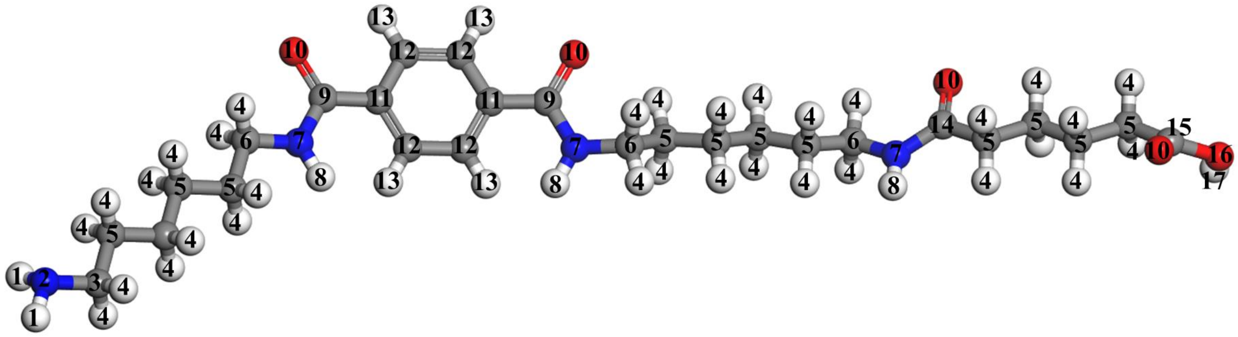

Figure S2: The distribution of atom in the PA6T/66 system. Blue, red, white and grey balls represent nitrogen, oxygen, hydrogen, and carbon atoms, respectively.

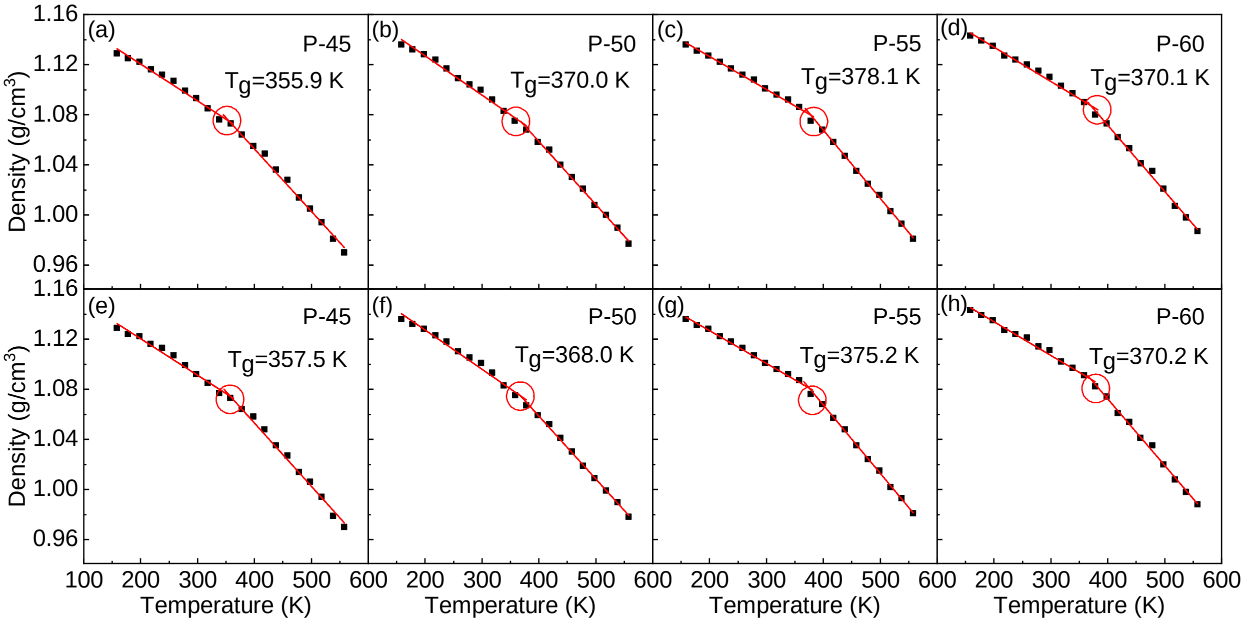

Figure S3: Density-temperature curves of P-45 (a, e), P-50 (b, f), P-55 (c, g), and P-60 (d, h), obtained from three independent simulations with a cooling rate of 10 K/ns. The red curve fits density in high-temperature and low-temperature regions, with their intersection marking the T_g.

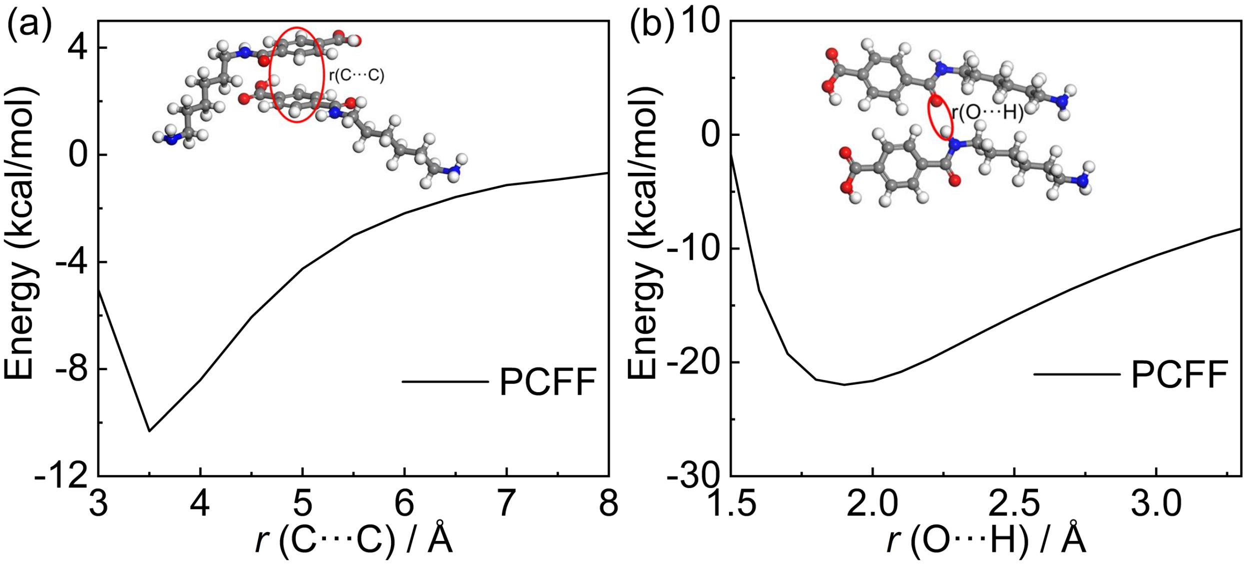

Figure S4: Intermolecular interactions in PA6T by the PCFF prediction. (a) π–π interactions, with the inset showing a schematic illustration of the molecular distance, and (b) hydrogen bonding interactions, with the inset showing a schematic illustration of the hydrogen bond distance.

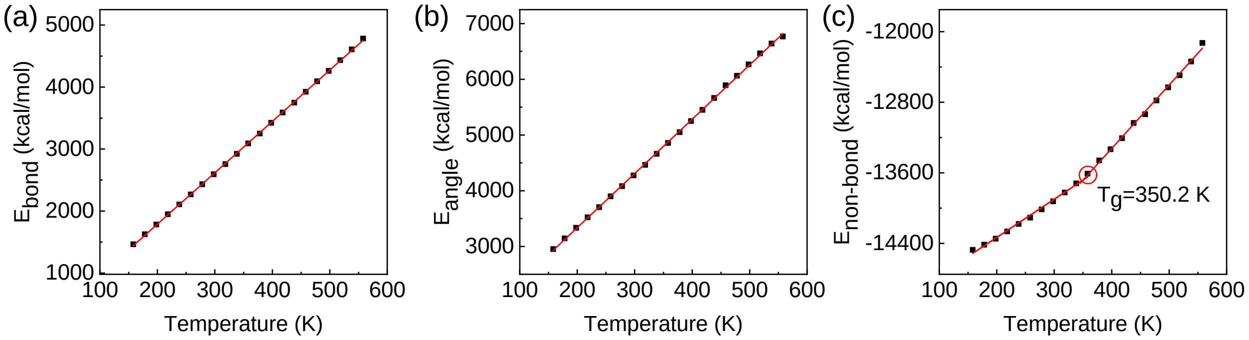

Figure S5: The component energies of the P-45 system at different temperatures. (a) Bond energy, corresponding to the energy associated with deviations from equilibrium bond lengths; (b) Angle energy, referring to the energy due to distortions in bond angles; and (c) Non-bonded interaction energy, encompassing van der Waals and electrostatic interactions between non-bonded atoms. All energy components are plotted as functions of simulation time at temperatures ranging from 158.15 K to 558.15 K.

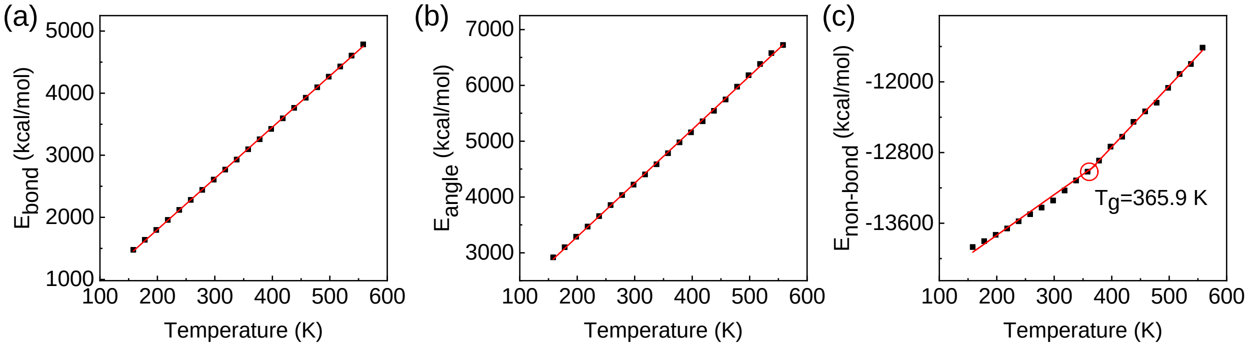

Figure S6: The component energies of the P-50 system at different temperatures. (a) Bond energy, corresponding to the energy associated with deviations from equilibrium bond lengths; (b) Angle energy, referring to the energy due to distortions in bond angles; and (c) Non-bonded interaction energy, encompassing van der Waals and electrostatic interactions between non-bonded atoms. All energy components are plotted as functions of simulation time at temperatures ranging from 158.15 K to 558.15 K.

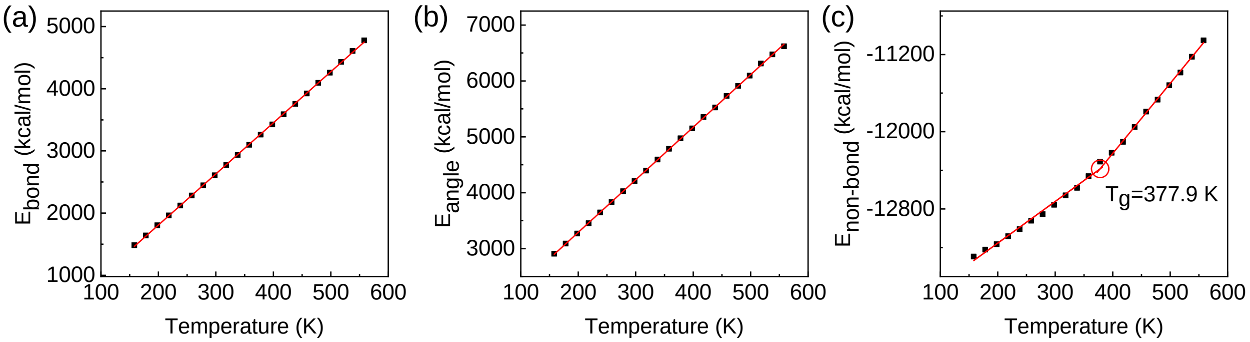

Figure S7: The component energies of the P-55 system at different temperatures. (a) Bond energy, corresponding to the energy associated with deviations from equilibrium bond lengths; (b) Angle energy, referring to the energy due to distortions in bond angles; and (c) Non-bonded interaction energy, encompassing van der Waals and electrostatic interactions between non-bonded atoms. All energy components are plotted as functions of simulation time at temperatures ranging from 158.15 K to 558.15 K.

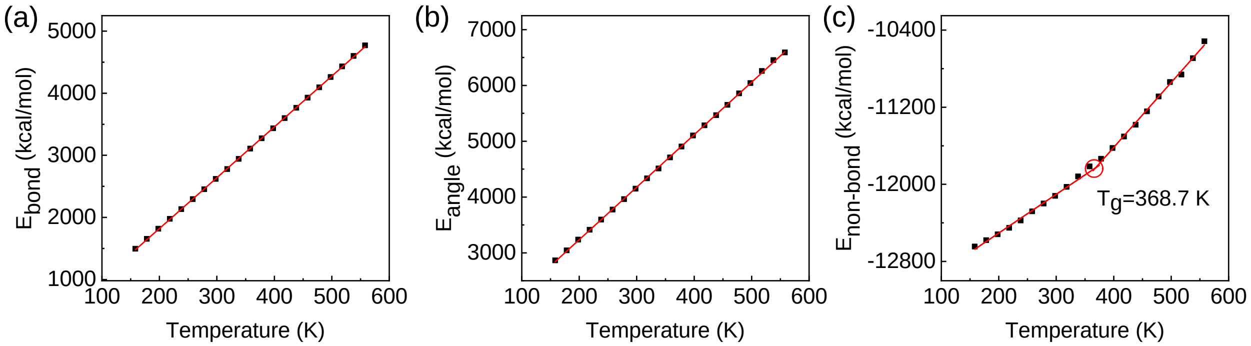

Figure S8: The component energies of the P-60 system at different temperatures. (a) Bond energy, corresponding to the energy associated with deviations from equilibrium bond lengths; (b) Angle energy, referring to the energy due to distortions in bond angles; and (c) Non-bonded interaction energy, encompassing van der Waals and electrostatic interactions between non-bonded atoms. All energy components are plotted as functions of simulation time at temperatures ranging from 158.15 K to 558.15 K.

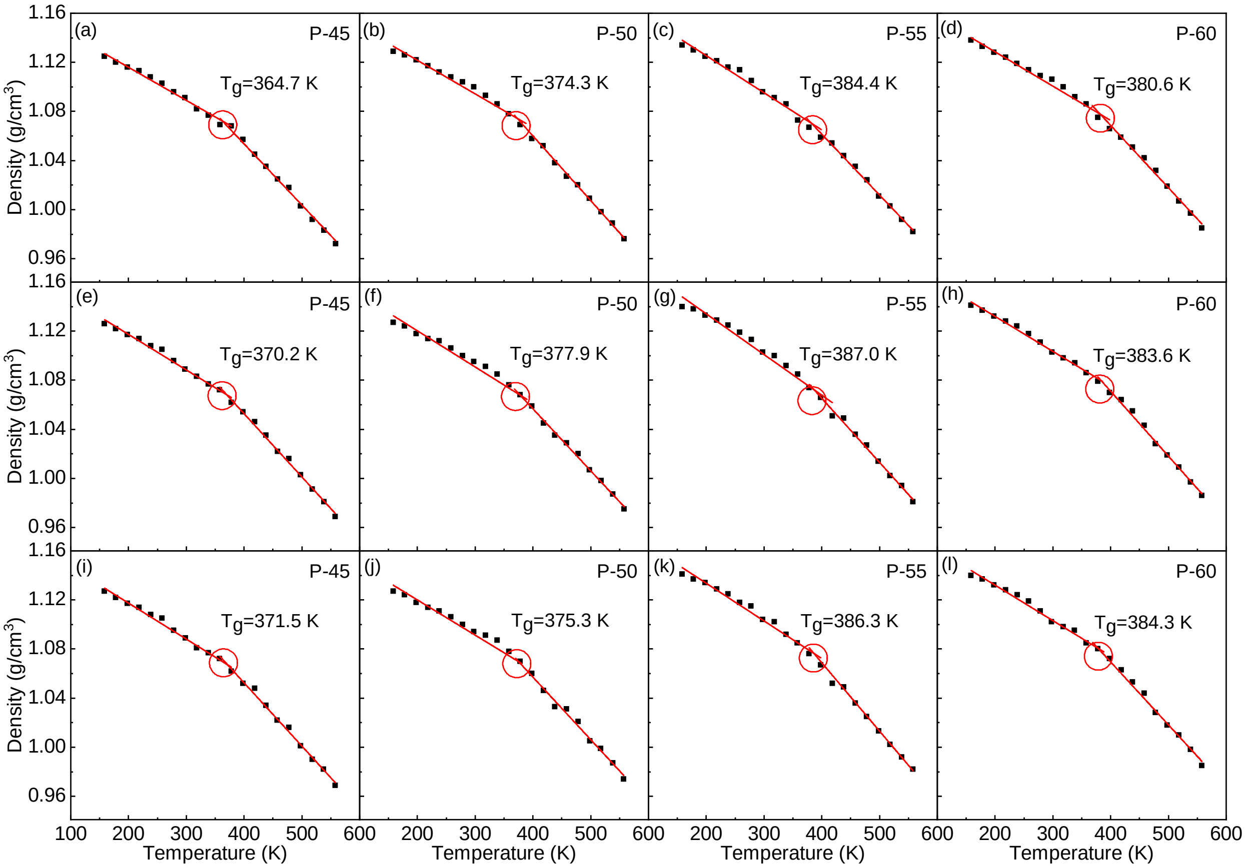

Figure S9: Density-temperature curves of P-45 (a, e, i), P-50 (b, f, j), P-55 (c, g, k), and P-60 (d, h, l), obtained from three independent simulations with a cooling rate of 20 K/ns. The red curve fits density in high-temperature and low-temperature regions, with their intersection marking the T_g.

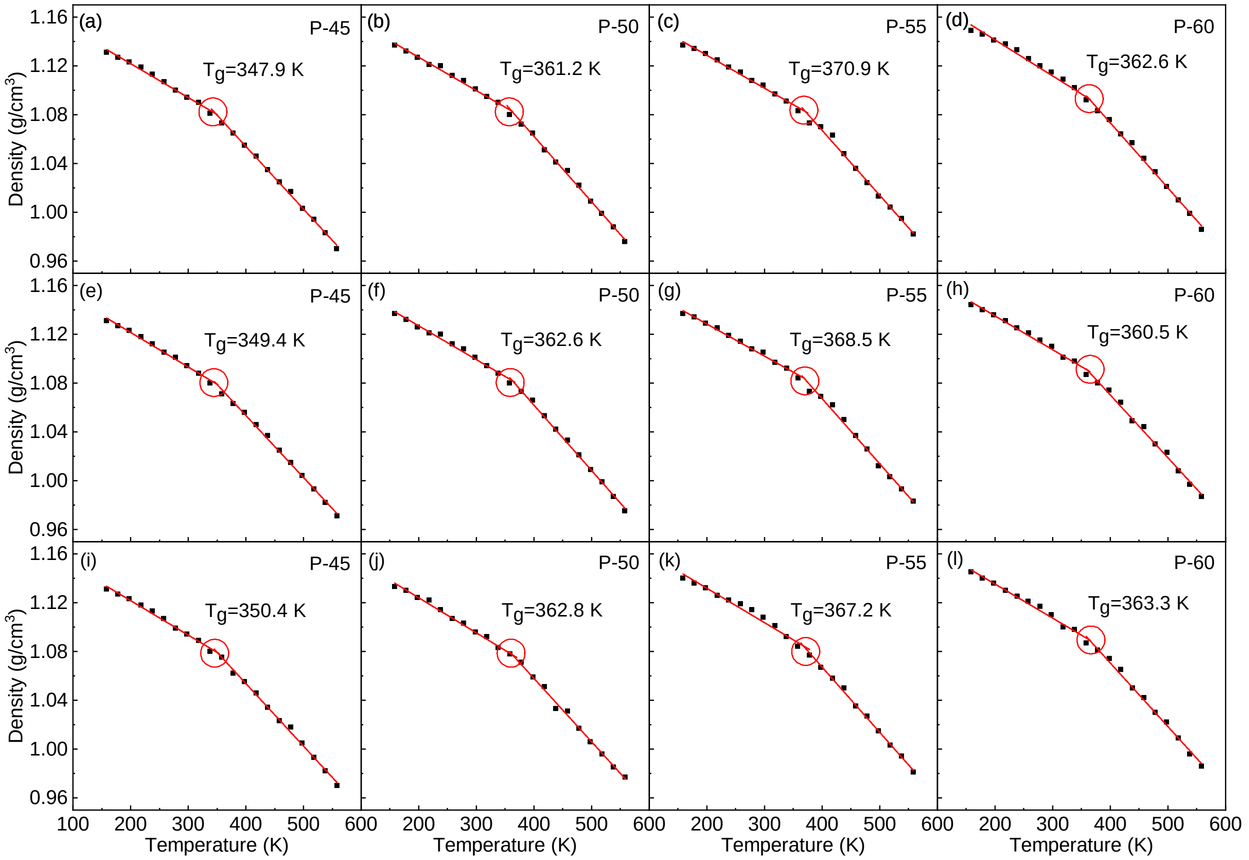

Figure S10: Density-temperature curves of P-45 (a, e, i), P-50 (b, f, j), P-55 (c, g, k), and P-60 (d, h, l), obtained from three independent simulations with a cooling rate of 5 K/ns. The red curve fits density in high-temperature and low-temperature regions, with their intersection marking the T_g, with a deviation of less than 10 K.

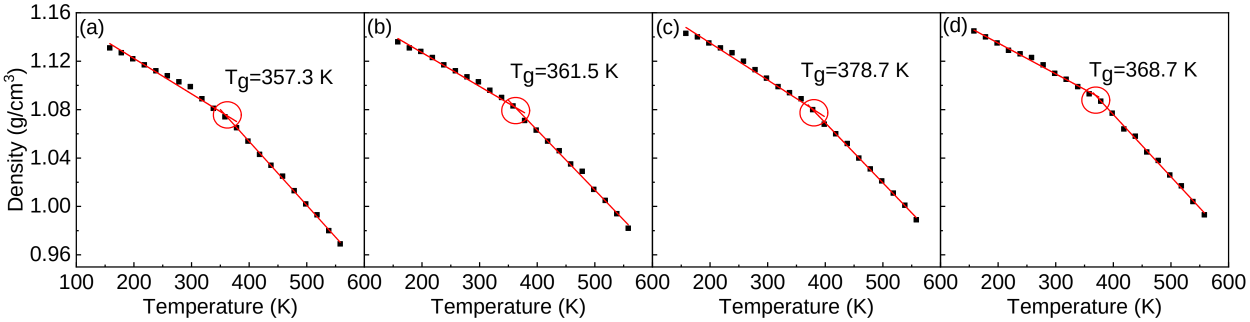

Figure S11: Density-temperature curves of block copolymers P-45 (a), P-50 (b), P-55 (c), and P-60 (d) with a cooling rate of 10 K/ns. The red curve fits density in high-temperature and low-temperature regions, with their intersection marking the T_g.

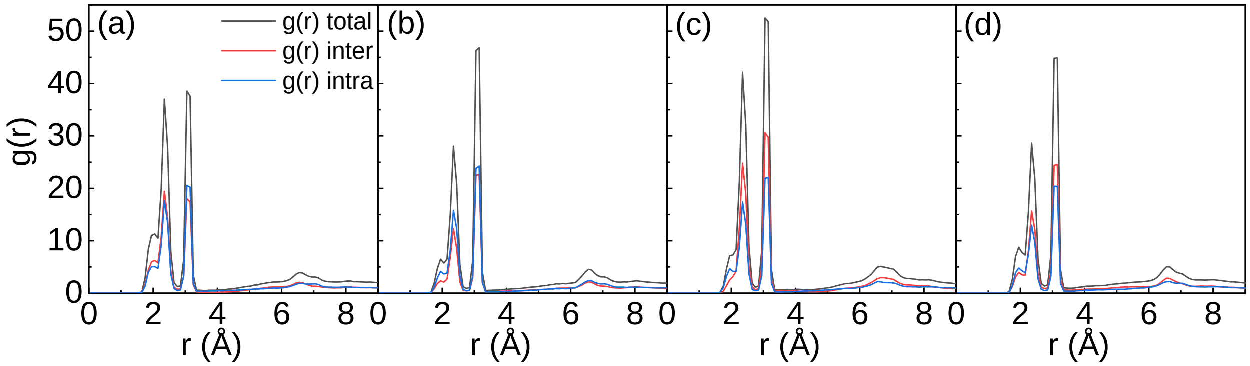

Figure S12: H-O radial distribution functions of P-45 (a), P-50 (b), P-55 (c), and P-60 (d) in 298.15 K.

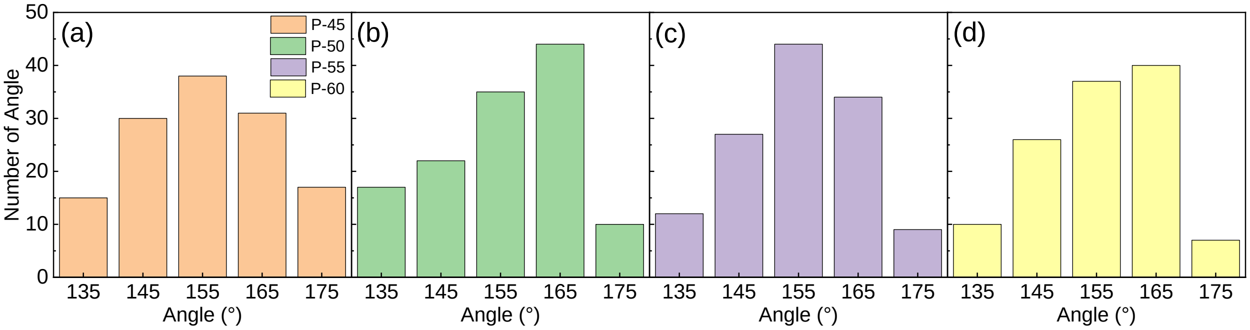

Figure S13: N-H. . . O angle distributions of P-45 (a), P-50 (b), P-55 (c), and P-60 (d) in 298.15 K.

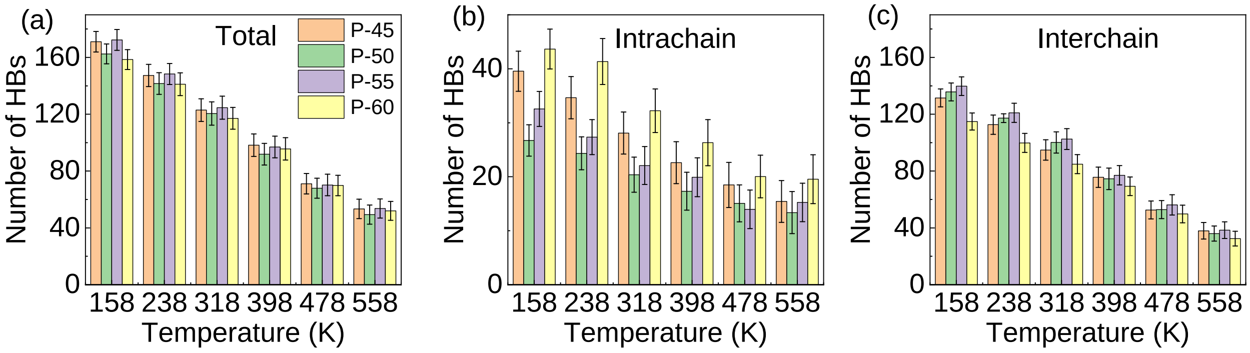

Figure S14: The number of total (a), intrachain (b), and interchain (c) HBs in P-45,P-50,P-55 and P-60 at different temperatures. The error bars are obtained by calculating the standard deviation, using the last 1000 frames of the equilibrated conforamtions with a time step of 1 ps.

Table S3: Energy distributions of the four systems at 158 K, 358 K, and 558 K.

System	Tempeature (K)	Bond energy (kcal/mol)	Angle Energy (kcal/mol)	van der Waals energy (kcal/mol)	Coulombic pairwise energy (kcal/mol)
P-45	158 K	1465.0	2950.7	-2848.0	15002.0
	358 K	3091.4	4855.5	-2314.4	15150.7
	558 K	4781.7	6766.7	-1485.3	16500.3
P-50	158 K	1476.5	2916.7	-2809.8	15587.4
	358 K	3094.9	4783.0	-2295.1	15740.2
	558 K	4784.6	6722.5	-1527.6	17152.4
P-55	158 K	1482.4	2905.9	-2747.5	16146.1
	358 K	3099.1	4785.3	-2227.7	16316.0
	558 K	4778.8	6620.2	-1494.7	17758.6
P-60	158 K	1494.2	2865.2	-2695.8	16790.9
	358 K	3107.4	4709.4	-2182.6	16913.5
	558 K	4771.3	6589.6	-1502.5	18359.0

Table S4: π-π stacking interaction energy selected with d less than 4 Å and α less than 20°, as illustrated in the inset of Fig. 6a, and hydrogen bond interaction energy for the P-45, P-50, P-55, and P-60 systems at 298.15 K.

System	non-bonded interaction (kcal/mol)	π-π interaction energy (kcal/mol)	hydrogen bond interaction energy (kcal/mol)
P-45	-13923.6	-41.2	-2900.0
P-50	-13343.8	-20.6	-2350.8
P-55	-12757.0	-20.6	-2922.0
P-60	-12120.2	-20.6	-2702.3

Table S5: Simulated T_g of P-45, P-50, P-55, and P-60 at cooling rates of 5 K/ns, 10 K/ns and 20 K/ns.

Cooling rate	P-45	P-50	P-55	P-60
5 K/ns	349.2 ($\pm$1.2) K	362.2 ($\pm$0.8) K	368.9 ($\pm$1.9) K	362.1 ($\pm$1.5) K
10 K/ns	356.3 ($\pm$1.1) K	368.6 ($\pm$1.2) K	376.8 ($\pm$1.5) K	370.8 ($\pm$1.1) K
20 K/ns	368.8 ($\pm$3.6) K	375.8 ($\pm$1.9) K	385.9 ($\pm$1.3) K	382.8 ($\pm$2.0) K